Nano Research 2018, 11(1): 323–333
https://doi.org/10.1007/s12274-017-1634-z
Research Article
ISSN 1998-0124
CN 11-5974/O4

Electrosynthesis of Co_3O_4 and $Co(OH)_2$ ultrathin nanosheet arrays for efficient electrocatalytic water splitting in alkaline and neutral media

Lin Zhang[1], Bingrui Liu[1], Ning Zhang[1,2] (✉), and Mingming Ma[1] (✉)

[1] *CAS Key Laboratory of Soft Matter Chemistry, iChEM (Collaborative Innovation Center of Chemistry for Energy Materials), Department of Chemistry, University of Science and Technology of China, Hefei 230026, China*
[2] *Department of Biology and Environmental Engineering, Hefei University, Hefei 230022, China*

Received: 28 February 2017
Revised: 23 March 2017
Accepted: 16 April 2017

KEYWORDS
electrosynthesis,
water splitting,
electrocatalysts,
non-noble metal,
ultrathin nanosheets

ABSTRACT

The dimensional confinement endows ultrathin nanosheets with unique physical and chemical properties, which have been widely studied for the purpose of developing active electrocatalysts for water splitting. Ultrathin nanosheets are generally synthesized by chemical vapor deposition, exfoliation, or surfactant-assisted synthesis, which either require special equipment and reaction conditions, or is limited by the low yields and the difficulty in controlling the lateral size and structure of the nanosheets. In addition, achieving a high loading of ultrathin nanosheets on the electrodes without compromising their catalytic activity still remains a challenge. Herein, we report a simple electrodeposition method for preparing Co_3O_4 and $Co(OH)_2$ ultrathin nanosheet arrays (UNA) without using templates or surfactants. The obtained arrays exhibit high activity for oxygen and hydrogen evolution reactions, in both alkaline and neutral media. The electrolyzer based on Co_3O_4 and $Co(OH)_2$ UNA shows superior activity and stability than that based on IrO_2 and Pt/C, which demonstrates the potential of the present electrodeposition method for developing active and stable electrocatalysts for water splitting.

1 Introduction

Electrochemical splitting of water into hydrogen and oxygen is an attractive way to store electricity from renewable energy sources in the form of clean chemical fuels [1]. The two half-reactions of water splitting, the hydrogen evolution reaction (HER) and the oxygen evolution reaction (OER), require active and robust electrocatalysts to facilitate the energy conversion process [2–4]. Noble-metal-based materials such as Pt [5] and IrO_2 [6] are highly active catalysts for HER or OER, but their high cost and low availability limit their large-scale applications. Therefore, materials based on non-noble metals [7] and carbon [8–9] have been

Address correspondence to Ning Zhang, zlab@ustc.edu.cn; Mingming Ma, mma@ustc.edu.cn

widely studied for the purpose of developing active electrocatalysts for water splitting. Particularly, many Co-based materials have been employed as active electrocatalysts, such as the OER catalysts $CoSe_2$ [10], Co_3O_4/N-doped reduced graphene oxide [11], γ-CoOOH [12], and β-CoOOH [13], and HER catalysts such as Co nanocrystals [14], CoP [15–16], CoS_2 [17–18], Co-S [19], MoS_2/$CoSe_2$ hybrids [20], as well as a few bifunctional OER/HER catalysts, such as Co-P-derived films [21], CoP mesoporous nanorod arrays [22], and NiCoP nanosheet arrays [23]. To further enhance the performance of these systems, several Co-based electrocatalysts with various micro- and nanostructures have been developed [24]. Among these structures, ultrathin nanosheets often show unique physical and chemical properties induced by the dimensional confinement. Therefore, several Co-based ultrathin nanosheets have been designed as active electrocatalyst for the HER [18, 20, 25] or OER [12, 26–28] processes. Ultrathin nanosheets are generally synthesized by chemical vapor deposition, exfoliation, or surfactant-assisted synthesis, which either require special equipment and reaction conditions, or are limited by the low yields and the difficulty in controlling the lateral size and structure of the nanosheets [29]. In addition, achieving high loadings of ultrathin nanosheets on the electrodes without compromising the catalytic activity of the nanosheets remains a significant challenge [12].

On the other hand, the electrosynthesis of active catalysts such as amorphous films [19, 21, 30], nanowire arrays [31–32], and nanosheet arrays [33–34] on the electrodes appears as a convenient approach for the rapid screening and large-scale production of electrocatalysts. For example, calcinations can be used to convert an array of $Co(OH)_2$ nanosheets electrodeposited on a substrate to another array of Co_3O_4 nanosheets [35–37], which can serve as active materials for supercapacitors [35, 37] or Li-ion batteries [36]. In this work, we propose an effective electrodeposition method to synthesize Co-based ultrathin nanosheets, vertically self-assembled on an electrode to form arrays, which can be used as active electrocatalysts for water splitting. These Co-based ultrathin nanosheet arrays (UNA) were prepared through a two-step procedure: A $Co_{0.85}Se$ film was first electrodeposited on Ni foam (NF) electrodes as the precursor, and then converted into crystalline Co_3O_4 or $Co(OH)_2$ UNA by anodic or cathodic reactions in 1 M KOH electrolyte (Scheme 1). In the conversion process, Se was sacrificed and replaced by the oxide or hydroxide. The UNA structures could be formed via a mechanism similar to that active for nanoporous anodic aluminum oxide [38], where the balance between localized dissolution of $Co_{0.85}Se$ and growth of Co_3O_4 or $Co(OH)_2$ leads to the formation of arrays of ultrathin nanosheets. Besides the large specific surface area and higher exposure of catalytic active sites resulting from the UNA structure [29], three additional desirable features are also achieved: Efficient mass transfer and charge transfer through the electrolyte, catalyst, and electrode; high loading of ultrathin nanosheets on the electrode, and efficient release of gas bubbles from the electrode surface. An electrolyzer assembled with Co_3O_4 UNA as OER catalyst and $Co(OH)_2$ UNA as HER catalyst showed high catalytic activity and stability in both alkaline and neutral media, superior to the performance of an electrolyzer based on Pt/C and IrO_2, which are the state-of-the-art electrocatalysts for water splitting [5–6].

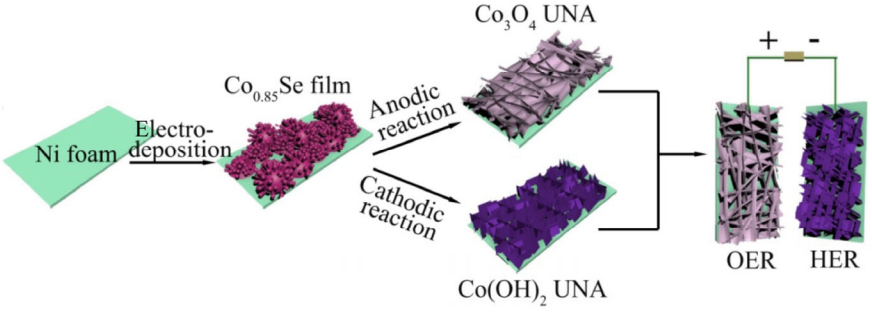

Scheme 1 Schematic illustration of the synthesis of Co_3O_4 and $Co(OH)_2$ ultrathin nanosheet arrays (UNA), and of their application as electrocatalysts for water splitting.

2 Experimental

2.1 Materials

IrO_2 and Pt/C (20 wt.% Pt) were purchased from Shanghai Macklin Biochemical Co., Ltd. and Alfa Aesar, respectively, and used as received. All other chemical reagents were of analytical grade; they were purchased from Sinopharm Chemical Reagent Co., Ltd. and used as received. Ni foam was obtained from Shanxi LZY Battery Material Co., Ltd. All solutions were prepared using deionized (DI) water.

2.2 Preparation of $Co_{0.85}Se$

$Co_{0.85}Se$ was electrodeposited on NF in a three-electrode configuration cell. A piece of NF (0.16 cm^2), a stainless steel plate (10 cm^2), and an Ag/AgCl (3.0 M KCl) electrode were used as working, counter, and reference electrode, respectively. Prior to the electrodeposition, NF was thoroughly rinsed with acetone, 0.5 M HCl, and then DI water. The aqueous deposition solution contains 65 mM $CoSO_4$, 35 mM SeO_2, and 200 mM K_2SO_4. Electrodeposition was performed at a constant potential of –0.65 V vs. Ag/AgCl for 1 h at room temperature. After electrodeposition, the as-prepared $Co_{0.85}Se$ on NF was rinsed three times with DI water.

The as-prepared amorphous Co alloy (Fig. S1 in the Electronic Supplementary Material (ESM)), was activated by electrochemical reduction in 1.0 M KOH at room temperature for 1 h, to give Co nanosheets vertically assembled on the NF electrode.

2.3 Preparation of Co_3O_4 UNA

The as-prepared $Co_{0.85}Se$ on NF was processed by anodic reaction in 1 M KOH electrolyte, at a constant potential of 0.7 V vs. Ag/AgCl for 1 h. The as-prepared Co_3O_4 UNA electrode was then rinsed three times with DI water. The loading amount of Co_3O_4 on the electrode was ~ 10 mg·cm^{-2}.

2.4 Preparation of $Co(OH)_2$ UNA

The as-prepared $Co_{0.85}Se$ on NF was processed by cathodic reaction in 1 M KOH electrolyte, at a constant potential of −1.4 V vs. Ag/AgCl for 1 h. The as-prepared $Co(OH)_2$ UNA electrode was then rinsed three times with distilled water. The loading amount of $Co(OH)_2$ on the electrode was ~ 8 mg·cm^{-2}.

2.5 Preparation of Pt/C and IrO_2 electrodes

A 10 mg amount of Pt/C or IrO_2 catalyst was dispersed in 2 mL ethanol by sonication for 30 min to form a homogeneous catalyst ink. Then, 32 μL of Pt/C or 64 μL of IrO_2 catalyst ink were drop-casted on the surface of NF (surface area 0.16 cm^2). The resulting electrode loadings were 1 mg·cm^{-2} for Pt/C and 2 mg·cm^{-2} for IrO_2.

2.6 Materials characterization

Before characterization, the as-prepared catalysts were washed three times with DI water and dried at room temperature. Powder X-Ray diffraction (XRD) was carried out on a TTR-III diffractometer with Cu Kα radiation (λ = 1.54178 Å). Scanning electron microscopy (SEM) was performed on a JSM-6700F instrument operated on 5.0 kV. Transmission electron microscopy (TEM) images were recorded on a JEOL-2010 microscope operating at 200 kV. X-ray photoelectron spectroscopy (XPS) measurements were performed with an ESCALAB 250 instrument, using Mg as the excitation source. Raman spectra were recorded by a LABRAM-HR system (λ = 514.5 nm). Atomic force microscopy (AFM) measurements were performed using a Cypher ES Environmental AFM. The loading of the catalysts was determined by inductively coupled plasma-atomic emission spectrometry (ICP-AES), using a Perkin-Elmer Corporation Optima 7300DV instrument. The N_2 adsorption isotherms were recorded on a BELSORP-max analyzer.

2.7 Electrochemical measurements

All electrocatalytic measurements were performed in a typical three-electrode configuration controlled by a CHI660E electrochemical workstation (CH Instruments, Inc.) with 1.0 M KOH or 1.0 M phosphate buffer solution (PBS) (pH = 7) as the electrolyte. A stainless steel sheet (10 cm^2) and an Ag/AgCl (in 3.0 M KCl solution) electrode were used as counter and reference electrode, respectively. Tafel and polarization curves were obtained at a scanning rate of 2 mV·s^{-1}. Electrochemical impedance spectroscopy (EIS) measurements

were performed at room temperature, over a 100 kHz–0.05 Hz frequency range at the amplitude of the sinusoidal voltage of 5 mV. The measured potentials vs. Ag/AgCl were converted to the reversible hydrogen electrode (RHE) scale using the relation E(RHE) = E(Ag/AgCl) + 0.059pH + 0.197. The HER overpotential (η) was assumed equal to E_{RHE}, whereas the OER overpotential was calculated as $\eta = E_{RHE} - 1.23$ V.

2.8 *iR* correction

In order to apply the ohmic drop correction, the contact resistance R_Ω was derived from the EIS data, which yielded typical values of 0.4–0.6 Ω·cm^2 for the tested catalysts on NF. The *iR* correction was calculated as $\eta_{corr} = \eta - jR_\Omega$, where η represents the applied overpotential, j is the current density, and R_Ω denotes the contact resistance.

2.9 Calculation of electrochemical double-layer capacitance

The electrochemically active surface area (ECAS) was calculated from the measured electrochemical double layer capacitance (C_{dl}) of the Co_3O_4 or $Co(OH)_2$ UNA electrode in 1.0 M neutral phosphate buffer (see ESM for details). Briefly, a potential range where no apparent Faradaic processes took place was determined using cyclic voltammetry (CV). The charging current $j_a - j_c$ was measured from the cyclic voltammograms at different scan rates, as shown in Figs. S12 and S21 in the ESM. According to the relation $j_a - j_c = 2\nu C_{dl}$ relation (where ν is the scan rate), C_{dl} can be estimated as the slope of a straight line plot of $j_a - j_c$ vs. ν.

3 Results and discussion

The $Co_{0.85}Se$ precursor to both Co_3O_4 and $Co(OH)_2$ UNA was deposited on NF through cathodic electrodeposition in an aqueous solution of $CoSO_4$ and SeO_2. The identity of $Co_{0.85}Se$ was confirmed by its power XRD pattern (Fig. S1 in the ESM), which matches that of hexagonal-phase $Co_{0.85}Se$ (JCPDS No. 52-1008) [39]. The Raman spectrum (Fig. S2 in the ESM) shows the characteristic peak of $Co_{0.85}Se$ at 182 cm^{-1} [40], whereas the XPS curves (Figs. S3(a) and S3(b) in the ESM) show the characteristic peaks corresponding to Co and Se. The two peaks at 782.1 and 798.1 eV in the Co 2p spectrum (Fig. S3(a) in the ESM) correspond to Co(II). The two broad peaks around 56 and 60 eV in the Se 3d spectrum (Fig. S3(b) in the ESM) are attributed to selenide ions in $Co_{0.85}Se$, and SeO_x species on the surface. The SEM images of $Co_{0.85}Se$ show a porous structure (Figs. S4(a) and S4(b) in the ESM), with a relatively low Brunauer–Emmett–Teller (BET) surface area of 6.75 m^2·g^{-1} (Fig. S5 in the ESM).

The $Co_{0.85}Se$-coated NF was electrochemically oxidized (0.7 V vs. Ag/AgCl) in 1 M KOH electrolyte to yield a product that was identified by XRD (Fig. S6 in the ESM) as Co_3O_4 (JCPDS No. 43-1003). The Raman spectrum of this product (Fig. S7 in the ESM) shows five bands characteristic of Co_3O_4 at 189, 463, 510, 604, and 667 cm^{-1} [41]. Figure 1(a) shows the SEM image of Co_3O_4 ultrathin nanosheets assembled together. Wrinkled nanosheets are clearly observed in the TEM image shown in Fig. 1(b). The corresponding selective area electron diffraction (SAED) pattern (inset of Fig. 1(b)) shows multiple discrete spots, which can be indexed to the (311), (222), and (440) fringes of cubic Co_3O_4.

The high resolution TEM (HRTEM) image in Fig. 1(c) shows that the Co_3O_4 nanosheets are mainly crystalline, with some amorphous regions. The well-resolved lattice fringe of 0.243 nm corresponds to the (311) fringe of cubic Co_3O_4. The AFM image (Fig. 1(d)) shows ultrathin nanosheets with an average thickness of 1.2 nm. The

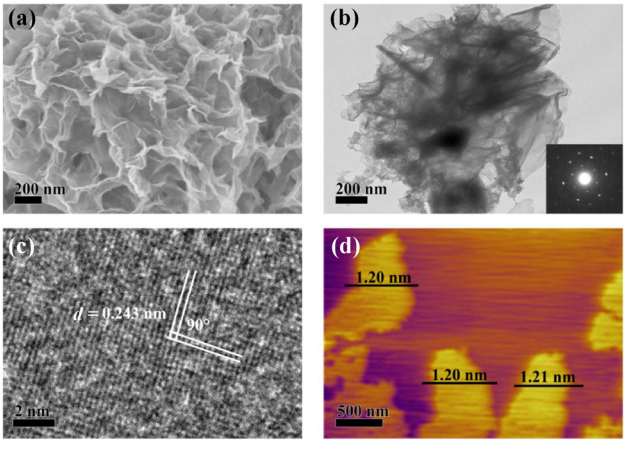

Figure 1 Characterization of Co_3O_4 UNA. (a) SEM image; (b) TEM image, with the SAED pattern in the inset; (c) HRTEM image showing the cubic spinel Co_3O_4 structure with the (311) plane exposed; (d) AFM image of Co_3O_4 ultrathin nanosheets.

two peaks at 780.3 and 796.7 eV in the Co 2p spectrum (Fig. S8 in the ESM) correspond to Co_3O_4 [11]. In addition, the BET surface area of the Co_3O_4 UNA (Fig. S9 in the ESM) was estimated as 158.85 $m^2 \cdot g^{-1}$, which is ~ 23 times larger than that of the precursor $Co_{0.85}Se$ (6.75 $m^2 \cdot g^{-1}$). The significantly enhanced surface area of Co_3O_4 is attributed to the large specific surface area of the ultrathin nanosheet structure, which becomes nanoporous (with pore size ~ 1 nm, Fig. S9 in the ESM) during the oxidation of $Co_{0.85}Se$.

The OER catalytic activity of the Co_3O_4 UNA (with a ~ 10 mg·cm^{-2} NF electrode loading) was first evaluated in a standard three-electrode system in 1.0 M KOH solution. For comparison, IrO_2 (~ 2 mg·cm^{-2}) was also loaded on NF and tested. As expected, bare NF showed poor OER activity (Fig. 2(a)). In contrast, the Co_3O_4 UNA can deliver 10 and 100 mA·cm^{-2} current densities at overpotentials of 148 and 268 mV, respectively, much lower than those of IrO_2 (296 and 368 mV) and superior to those reported for most non-noble OER electrocatalysts in alkaline media (Table S1 in the ESM). Moreover, with a low overpotential of 340 mV, the Co_3O_4 UNA can achieve a remarkable current density of 980 mA·cm^{-2} in alkaline media. As shown in Fig. 2(b), the Tafel slope of Co_3O_4 UNA (48 mV·dec^{-1}) was smaller than that of IrO_2 (63 mV·dec^{-1}). The Nyquist plots show that the charge transfer resistance (R_{ct}) measured for the Co_3O_4 UNA is 0.02 Ω·cm^2, which is much lower than that of IrO_2 (0.6 Ω·cm^2, Fig. S10 in the ESM). A previous study has shown that the Co_3O_4 UNA have a very high density of states at the conduction band edge, leading to good electric conductivity [42]. Both the low Tafel slope and low R_{ct} of the Co_3O_4 UNA can thus be attributed to the high conductivity of Co_3O_4 ultrathin nanosheets and their efficient electrical contact with NF.

Besides alkaline media, the OER catalytic activity of the Co_3O_4 UNA was also tested in neutral media (1.0 M PBS, pH = 7), because the latter are environmentally benign and can efficiently prevent corrosion. In neutral media, the Co_3O_4 UNA exhibit much better catalytic performance than IrO_2 and bare NF (Fig. 2(d)). The Co_3O_4 UNA can deliver current densities of 10 and 50 mA·cm^{-2} at overpotentials of 207 and 379 mV, respectively, which are much lower than those of IrO_2 (389 and 683 mV) and also superior to those reported for most non-noble OER electrocatalysts in neutral media (Table S2 in the ESM). As shown in Fig. 2(e), the

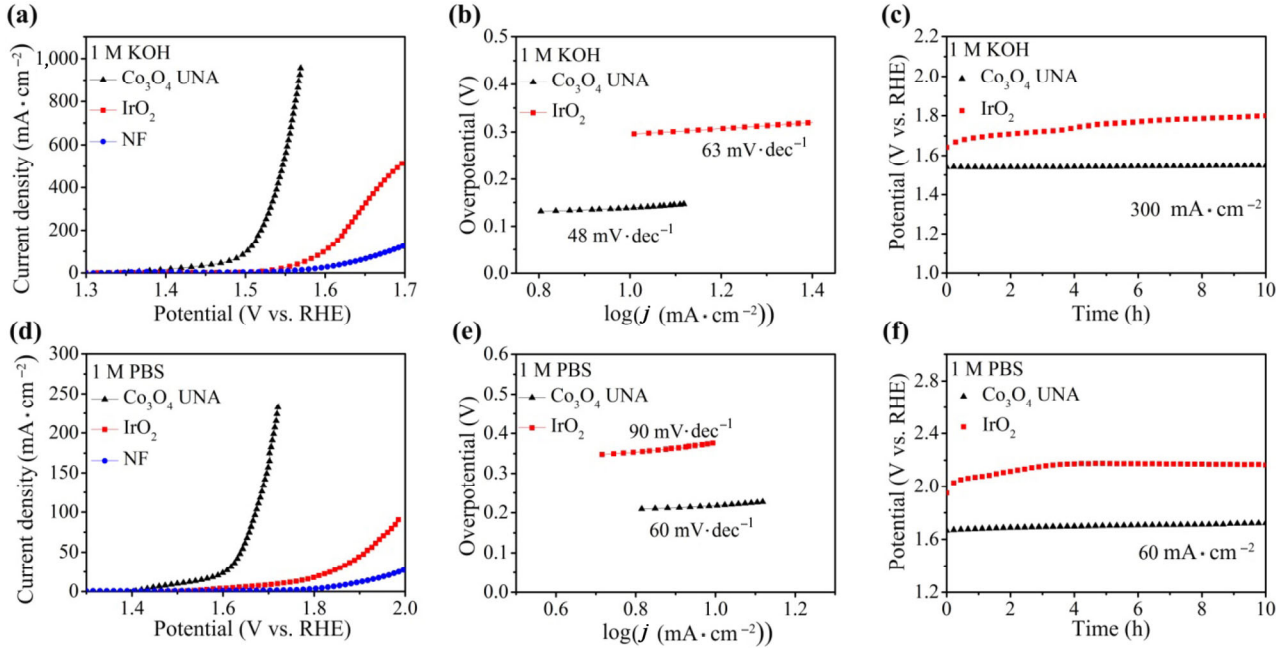

Figure 2 Electrocatalytic OER in 1 M KOH and 1 M PBS (pH = 7) electrolytes. (a), (d) OER polarization curves of Co_3O_4 UNA (black), IrO_2 (red), and NF (blue) at a scan rate of 2 mV·s^{-1}, and (b), (e) corresponding Tafel plots. (c), (f) Chronopotentiometry curves of Co_3O_4 UNA (black) and IrO_2 (red) under a current density of 300 mA·cm^{-2} in 1 M KOH and 60 mA·cm^{-2} in 1 M PBS electrolytes, respectively. All polarization curves were *iR*-corrected.

measured Tafel slope of the Co_3O_4 UNA (60 mV·dec^{-1}) was smaller than that of IrO_2 (90 mV·dec^{-1}). The Nyquist plots show that the R_{ct} of the Co_3O_4 UNA is 0.6 Ω·cm^2, which is much lower than that of IrO_2 (30 Ω·cm^2, Fig. S11 in the ESM).

The outstanding catalytic activity of the Co_3O_4 UNA in both alkaline and neutral media is attributed to the UNA structure, which exhibits a large active surface area and enables a high electrode loading of ultrathin nanosheets without compromising their catalytic activity. The active surface area of the Co_3O_4 UNA was estimated by measuring their electrochemical double layer capacitance [43]. Owing to the high Co_3O_4 UNA loading on NF and to the UNA structure, the C_{dl} of the Co_3O_4 UNA electrode was estimated at 0.16 F·cm^{-2} in neutral media (Fig. S12 in the ESM), which indicates a large electrochemical active surface area and accounts for its high OER activity.

The durability of the Co_3O_4 UNA as OER catalysts was tested by performing long-term OER tests in both alkaline and neutral media, and compared with the durability of IrO_2. The Co_3O_4 UNA and IrO_2 electrodes were first tested in alkaline media, at a high current density of 300 mA·cm^{-2} for 10 h. The driving potential of the Co_3O_4 UNA electrode remained constant at 1.54 V, while that of the IrO_2 electrode gradually increased from 1.64 to 1.79 V (Fig. 2(c)). The electrodes were then tested in neutral media, at a current density of 60 mA·cm^{-2} for 10 h. Again, the driving potential of the Co_3O_4 UNA electrode remained constant at 1.67 V, while that of the IrO_2 electrode gradually increased from 1.95 to 2.17 V (Fig. 2(f)). The XRD and Raman spectra (Figs. S13(a) and S13(b) in the ESM) show that the structure of the Co_3O_4 UNA remains unchanged after the OER tests in either alkaline or neutral media. The long-term OER test and the subsequent structure characterization clearly demonstrate the superior stability of the Co_3O_4 UNA electrode in the OER process under heavy loading conditions, both in alkaline and neutral media.

Having established the high activity and stability of Co_3O_4 UNA in the OER process, we need to identify a HER catalyst with similar high performance. Again, we used $Co_{0.85}Se$ as the precursor and converted it to $Co(OH)_2$ by cathodic reaction. A cathodic potential (−1.4 V vs. Ag/AgCl) was applied on the $Co_{0.85}Se$-coated NF in 1.0 M KOH as electrolyte, to yield a product that was identified by XRD (Fig. S14 in the ESM) as $Co(OH)_2$ (JCPDS No. 30-0443). The Raman spectrum (Fig. S15 in the ESM) shows four bands characteristic of $Co(OH)_2$ at 191, 463, 519, and 689 cm^{-1} [44-45]. The IR spectrum of $Co(OH)_2$ is shown in Fig. S16 of the ESM, with a sharp peak at 3626 cm^{-1} attributed to the O–H stretching vibration, and a band at about 670 cm^{-1} assigned to the Co–OH vibration [46]. The SEM image in Fig. 3(a) shows that the $Co(OH)_2$ UNA are porous and spatially interconnected. A wrinkled nanosheet structure was highlighted by TEM (Fig. 3(b)), while the corresponding SAED pattern (inset of Fig. 3(b)) shows discrete spots corresponding to the (100) and (110) fringes of $Co(OH)_2$. The HRTEM image in Fig. 3(c) shows that the $Co(OH)_2$ UNA are characterized by clear lattice fringes with interplanar spacing of 0.237 nm corresponding to the (101) plane of $Co(OH)_2$. The AFM image (Fig. 3(d)) shows ultrathin nanosheets with an average thickness of 1.4 nm. The XPS in the Co 2p region is shown in Fig. S17 of the ESM. The two peaks at 781.9 and 798.0 eV are assigned to $Co(OH)_2$. In addition, the BET surface area of the $Co(OH)_2$ UNA (Fig. S18 in the ESM) was 16.72 m^2·g^{-1}, which is ~ 2.4 times higher than that of the $Co_{0.85}Se$ precursor (6.75 m^2·g^{-1}).

The HER catalytic activity of the $Co(OH)_2$ UNA (with a ~ 8 mg·cm^{-2} NF electrode loading) was evaluated in a standard three-electrode system. For comparison, Pt/C (~ 1 mg·cm^{-2} loading) was also loaded on NF and tested for comparison. Bare NF exhibited poor HER activity in both alkaline and neutral media, while the Pt/C electrode showed excellent HER activity, with an onset overpotential of ~ 0 mV (Figs. 4(a) and 4(d)). In alkaline media, the $Co(OH)_2$ UNA electrode delivered current densities of 10, 100, and 300 mA·cm^{-2} at overpotentials of 46, 171, and 224 mV, respectively. These performances are superior to those of most non-noble metal HER catalysts in alkaline electrolytes (Table S3 in the ESM). The Tafel slope measured for $Co(OH)_2$ UNA was 85 mV·dec^{-1}, which is close to that of Pt/C (67 mV·dec^{-1}, Fig. 4(b)). The Nyquist plots (Fig. S19 in the ESM) highlight a low charge transfer resistance (R_{ct}) of $Co(OH)_2$ UNA (5.0 Ω·cm^2), comparable to that of Pt/C (3.0 Ω·cm^2). In neutral media (1 M PBS, pH = 7), the $Co(OH)_2$ UNA electrode

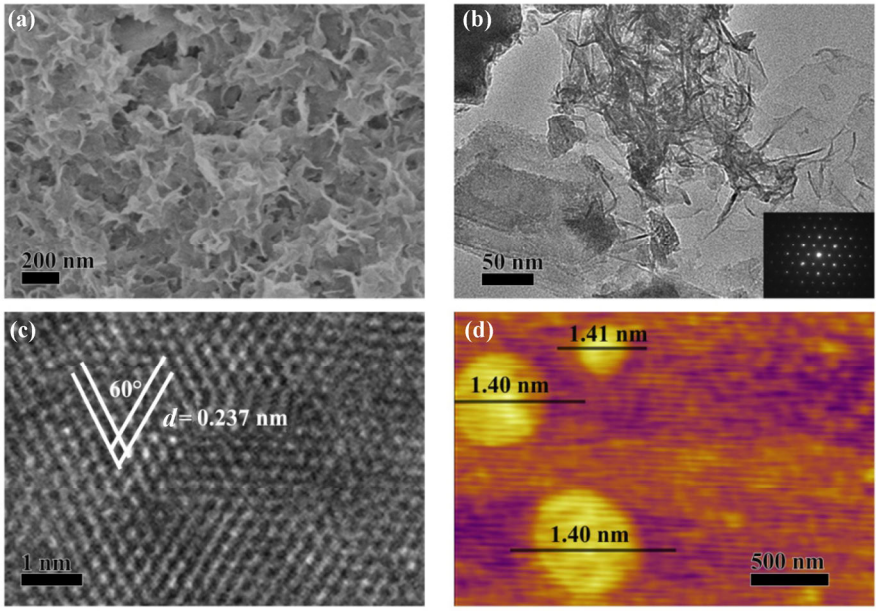

Figure 3 Characterization of $Co(OH)_2$ UNA. (a) SEM image; (b) TEM image (the inset shows the SAED pattern); (c) HRTEM image showing the hexagonal $Co(OH)_2$ phase with the (101) plane exposed; (d) AFM image of $Co(OH)_2$ ultrathin nanosheets.

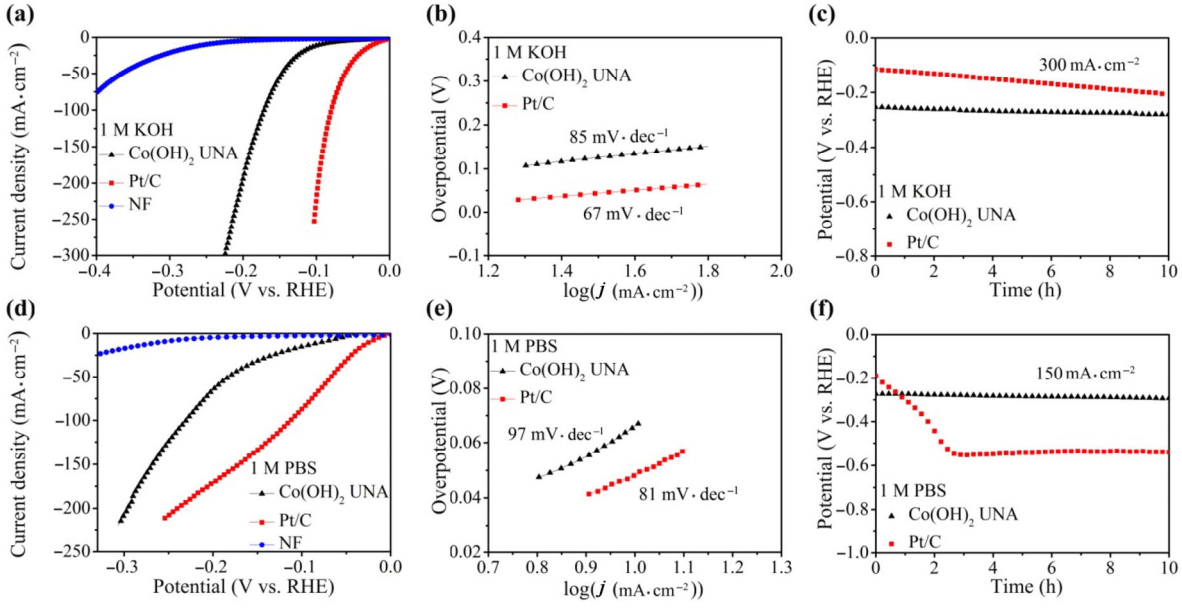

Figure 4 Electrocatalytic HER in 1 M KOH and 1 M PBS electrolytes. (a), (d) HER polarization curves of $Co(OH)_2$ UNA (black), Pt/C (red), and NF (blue) at a scan rate of 2 $mV \cdot s^{-1}$, and (b), (e) corresponding Tafel plots. (c), (f) Chronopotentiometry curves of $Co(OH)_2$ UNA (black) and Pt/C (red) under a current density of 300 $mA \cdot cm^{-2}$ in 1 M KOH and 150 $mA \cdot cm^{-2}$ in 1 M PBS electrolytes, respectively. All polarization curves were *iR*-corrected.

delivered current densities of 10, 100, and 200 $mA \cdot cm^{-2}$ at overpotentials of 70, 240, and 289 mV, respectively, again with performances superior to those of most non-noble HER metal catalysts in neutral electrolytes (Table S4 in the ESM). The Tafel slope measured for $Co(OH)_2$ UNA was 97 $mV \cdot dec^{-1}$, close to that of Pt/C (81 $mV \cdot dec^{-1}$, Fig. 4(e)). The Nyquist plots (Fig. S20 in the ESM) highlight a low charge transfer resistance (R_{ct}) of the $Co(OH)_2$ UNA (6.5 $\Omega \cdot cm^2$), comparable to that of Pt/C (3.9 $\Omega \cdot cm^2$). The C_{dl} measured for the $Co(OH)_2$ UNA electrode was 0.35 $F \cdot cm^{-2}$ in neutral media (Fig. S21 in the ESM), which indicates a large

electrochemical active surface area and accounts for its high HER activity.

The durability of the $Co(OH)_2$ UNA in the HER process was tested by long-term HER tests at constant currents of 150 $mA·cm^{-2}$ in neutral electrolyte and 300 $mA·cm^{-2}$ in alkaline electrolyte, and compared with the corresponding performance of the Pt/C catalyst. The catalytic activity of the $Co(OH)_2$ UNA was very stable during 10-h-long HER tests in both alkaline and neutral media (Figs. 4(c) and 4(f)). In contrast, Pt/C exhibits lower durability compared with $Co(OH)_2$ UNA, with a clear decay in its catalytic activity during the long-term HER test. In particular, in neutral media the Pt/C electrode initially required a smaller potential of –190 mV, which rapidly changed to −552 mV after 3 h, and then remained around −530 mV for the rest of the test. The fast deactivation of the Pt/C catalyst at high current densities in neutral media was attributed to the aggregation of Pt nanoparticles during the HER process, as indicated by the TEM images (Fig. S22 in the ESM). In contrast, the $Co(OH)_2$ UNA electrode retained the driving potential of −285 mV in neutral media. This comparison clearly demonstrates the superior electrocatalytic stability of $Co(OH)_2$ UNA over Pt/C under heavy-loading operating condition in both neutral and alkaline media. The XRD and Raman spectra (Figs. S23(a) and S23(b) in the ESM) show that the structure of the $Co(OH)_2$ UNA remains unchanged after the HER tests in either alkaline or neutral media. The long-term HER tests and subsequent structure characterization thus confirm the superior stability of the $Co(OH)_2$ UNA electrode in the HER process under heavy loading conditions, in both alkaline and neutral media.

The performances of an electrocatalyst are often disrupted by the evolution of H_2 or O_2 bubbles, which tend to stick to the electrode surface and limit the active surface area and mass transport [47]. Both Co_3O_4 and $Co(OH)_2$ UNA possess a hydrophilic surface and a vertically assembled nanosheets structure, which can facilitate the fast release of O_2 or H_2 as tiny bubbles [48]. Therefore, the Co_3O_4 and $Co(OH)_2$ UNA electrodes can produce high current densities at low overpotential without electrode rotation or solution stirring, which favor their practical application to water splitting.

Having established the high activity and stability of the individual electrodes for water splitting reactions, we prepared an electrolytic cell using the Co_3O_4 and $Co(OH)_2$ UNA as anode and cathode, respectively. Two electrolyzers, based on IrO_2‖Pt/C and NF‖NF couples, were also assembled and tested for comparison. In alkaline media, the Co_3O_4 UNA‖ $Co(OH)_2$ UNA electrolyzer can attain current densities of 10 and 50 $mA·cm^{-2}$ at voltages of 1.41 and 1.69 V, respectively, much lower than those measured for the IrO_2‖Pt/C electrolyzer (1.62 and 1.85 V, Fig. 5(a)). In neutral media, the polarization curve of the Co_3O_4 UNA‖$Co(OH)_2$ UNA electrolyzer almost coincided with that of the IrO_2‖Pt/C electrolyzer in the low voltage region, and exceeded it in the high voltage region (Fig. 5(c)). The comparison thus demonstrates the superior water splitting activity of the Co_3O_4 UNA‖$Co(OH)_2$ UNA electrolyzer in both alkaline and neutral media. In addition, the long-term durability of this electrolyzer was also tested at current densities of 120 and 60 $mA·cm^{-2}$ in alkaline and neutral media, respectively (Figs. 5(b) and 5(d)). Under both conditions, the Co_3O_4 UNA‖$Co(OH)_2$ UNA electrolyzer required a lower driving voltage than the IrO_2‖Pt/C one during a 10 h water splitting test, which further demonstrates the superior activity and durability of the Co_3O_4 UNA‖$Co(OH)_2$ UNA electrolyzer.

4 Conclusions

In summary, we have developed a facile electrochemical method to synthesize Co-based ultrathin nanosheet arrays as efficient and robust electrocatalysts for water splitting in both alkaline and neutral media. The Co_3O_4 and $Co(OH)_2$ UNA can be employed as electrocatalysts for the OER and HER processes, respectively; they can drive large current densities at a low overpotential and deliver stable operation under heavy loading conditions over an extended period. The Co_3O_4 UNA‖$Co(OH)_2$ UNA electrolyzer shows high catalytic activity and stability for water splitting in both alkaline and neutral media, exceeding that of the IrO_2‖Pt/C electrolyzer, and is among the best non-noble electrocatalyst for overall water splitting. In addition, the Co_3O_4 and $Co(OH)_2$ UNA electrocatalysts can be facilely synthesized in only 3 h using an electrochemical

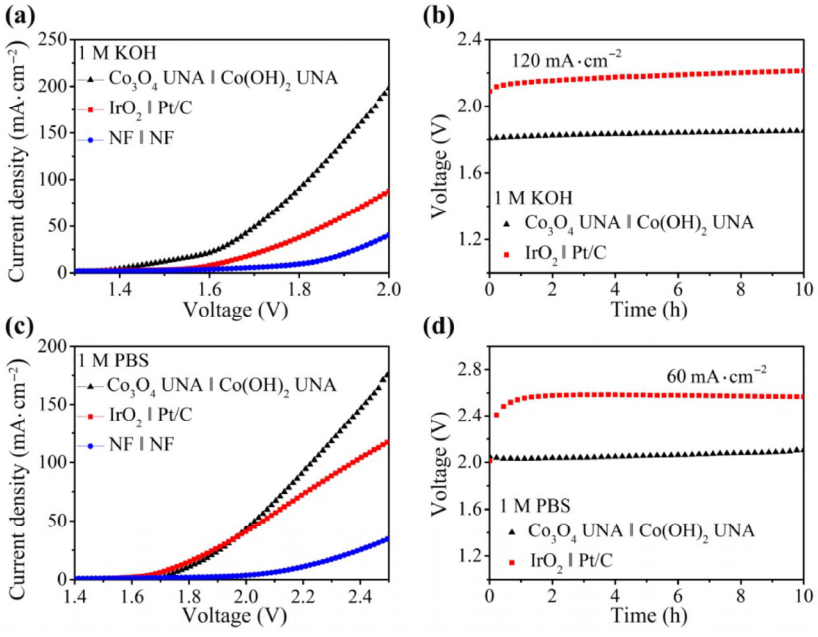

Figure 5 Electrocatalytic water splitting in 1 M KOH and 1 M PBS electrolytes. (a), (c) Polarization curves of electrolyzers based on Co_3O_4 UNA ‖ $Co(OH)_2$ UNA (black), IrO_2 ‖ Pt/C (red), and NF ‖ NF (blue) cells, with a scan rate of 2 mV·s^{-1}. (b), (d) Chronopotentiometry curves of electrolyzers based on Co_3O_4 UNA ‖ $Co(OH)_2$ UNA (black) and IrO_2 ‖ Pt/C (red) cells with current densities of 120 mA·cm^{-2} in 1 M KOH and 60 mA·cm^{-2} in 1 M PBS electrolytes, respectively.

workstation and a simple wet-chemical procedure, which demonstrates that the present electrodeposition method is suitable for preparing electrocatalysts with an ultrathin nanosheet array structure.

Acknowledgements

This work was supported by the National Natural Science Foundation of China (Nos. 21474094 and 81401531) and the Natural Science Foundation of Anhui Province (No. 1508085QH154).

Electronic Supplementary Material: Supplementary material (characterization and electrochemical tests of Co_3O_4 UNA and $Co(OH)_2$ UNA) is available in the online version of this article at https://doi.org/10.1007/s12274-017-1634-z.

References

[1] Thoi, V. S.; Sun, Y. J.; Long, J. R.; Chang, C. J. Complexes of earth-abundant metals for catalytic electrochemical hydrogen generation under aqueous conditions. *Chem. Soc. Rev.* **2013**, *42*, 2388–2400.

[2] Nocera, D. G. The artificial leaf. *Acc. Chem. Res.* **2012**, *45*, 767–776.

[3] Joya, K. S.; Joya, Y. F.; Ocakoglu, K.; Van de Krol, R. Water-splitting catalysis and solar fuel devices: Artificial leaves on the move. *Angew. Chem., Int. Ed.* **2013**, *52*, 10426–10437.

[4] Jiao, Y.; Zheng, Y.; Jaroniec, M.; Qiao, S. Z. Design of electrocatalysts for oxygen- and hydrogen-involving energy conversion reactions. *Chem. Soc. Rev.* **2015**, *44*, 2060–2086.

[5] Greeley, J.; Jaramillo, T. F.; Bonde, J.; Chorkendorff, I. B.; Nørskov, J. K. Computational high-throughput screening of electrocatalytic materials for hydrogen evolution. *Nat. Mater.* **2006**, *5*, 909–913.

[6] Frame, F. A.; Townsend, T. K.; Chamousis, R. L.; Sabio, E. M.; Dittrich, T.; Browning, N. D.; Osterloh, F. E. Photocatalytic water oxidation with nonsensitized IrO_2 nanocrystals under visible and UV light. *J. Am. Chem. Soc.* **2011**, *133*, 7264–7267.

[7] Kong, D. S.; Cha, J. J.; Wang, H. T.; Lee, H. R.; Cui, Y. First-row transition metal dichalcogenide catalysts for hydrogen evolution reaction. *Energy Environ. Sci.* **2013**, *6*, 3553–3558.

[8] Zhao, Y.; Zhao, F.; Wang, X. P.; Xu, C. Y.; Zhang, Z. P.; Shi, G. Q.; Qu, L. T. Graphitic carbon nitride nanoribbons: Graphene-assisted formation and synergic function for highly efficient hydrogen evolution. *Angew. Chem., Int. Ed.* **2014**, *53*, 13934–13939.

[9] Liu, Z. Y.; Zhang, G. X.; Lu, Z. Y.; Jin, X. Y.; Chang, Z.; Sun, X. M. One-step scalable preparation of N-doped nanoporous carbon as a high-performance electrocatalyst for the oxygen reduction reaction. *Nano Res.* **2013**, *6*, 293–301.

[10] Liang, L.; Cheng, H.; Lei, F. C.; Han, J.; Gao, S.; Wang, C. M.; Sun, Y. F.; Qamar, S.; Wei, S. Q.; Xie, Y. Metallic single-unit-cell orthorhombic cobalt diselenide atomic layers: Robust water-electrolysis catalysts. *Angew. Chem., Int. Ed.* **2015**, *54*, 12004–12008.

[11] Liang, Y. Y.; Li, Y. G.; Wang, H. L.; Zhou, J. G.; Wang, J.; Regier, T.; Dai, H. J. Co_3O_4 nanocrystals on graphene as a synergistic catalyst for oxygen reduction reaction. *Nat. Mater.* **2011**, *10*, 780–786.

[12] Huang, J. H.; Chen, J. T.; Yao, T.; He, J. F.; Jiang, S.; Sun, Z. H.; Liu, Q. H.; Cheng, W. R.; Hu, F. C.; Jiang, Y. et al. CoOOH nanosheets with high mass activity for water oxidation. *Angew. Chem., Int. Ed.* **2015**, *54*, 8722–8727.

[13] Bajdich, M.; García-Mota, M.; Vojvodic, A.; Nørskov, J. K.; Bell, A. T. Theoretical investigation of the activity of cobalt oxides for the electrochemical oxidation of water. *J. Am. Chem. Soc.* **2013**, *135*, 13521–13530.

[14] Liu, B. R.; Zhang, L.; Xiong, W. L.; Ma, M. M. Cobalt-nanocrystal-assembled hollow nanoparticles for electrocatalytic hydrogen generation from neutral-pH water. *Angew. Chem., Int. Ed.* **2016**, *55*, 6725–6729.

[15] Popczun, E. J.; Read, C. G.; Roske, C. W.; Lewis, N. S.; Schaak, R. E. Highly active electrocatalysis of the hydrogen evolution reaction by cobalt phosphide nanoparticles. *Angew. Chem., Int. Ed.* **2014**, *53*, 5427–5430.

[16] Tian, J. Q.; Liu, Q.; Asiri, A. M.; Sun, X. P. Self-supported nanoporous cobalt phosphide nanowire arrays: An efficient 3D hydrogen-evolving cathode over the wide range of pH 0–14. *J. Am. Chem. Soc.* **2014**, *136*, 7587–7590.

[17] Faber, M. S.; Dziedzic, R.; Lukowski, M. A.; Kaiser, N. S.; Ding, Q.; Jin, S. High-performance electrocatalysis using metallic cobalt pyrite (CoS_2) micro-and nanostructures. *J. Am. Chem. Soc.* **2014**, *136*, 10053–10061.

[18] Peng, S. J.; Li, L. L.; Han, X. P.; Sun, W. P.; Srinivasan, M.; Mhaisalkar, S. G.; Cheng, F. Y.; Yan, Q. Y.; Chen, J.; Ramakrishna, S. Cobalt sulfide nanosheet/graphene/carbon nanotube nanocomposites as flexible electrodes for hydrogen evolution. *Angew. Chem., Int. Ed.* **2014**, *53*, 12594–12599.

[19] Sun, Y. J.; Liu, C.; Grauer, D. C.; Yano, J.; Long, J. R.; Yang, P. D.; Chang, C. J. Electrodeposited cobalt-sulfide catalyst for electrochemical and photoelectrochemical hydrogen generation from water. *J. Am. Chem. Soc.* **2013**, *135*, 17699–17702.

[20] Gao, M. R.; Liang, J. X.; Zheng, Y. R.; Xu, Y. F.; Jiang, J.; Gao, Q.; Li, J.; Yu, S. H. An efficient molybdenum disulfide/cobalt diselenide hybrid catalyst for electrochemical hydrogen generation. *Nat. Commun.* **2015**, *6*, 5982.

[21] Jiang, N.; You, B.; Sheng, M. L.; Sun, Y. J. Electrodeposited cobalt-phosphorous-derived films as competent bifunctional catalysts for overall water splitting. *Angew. Chem., Int. Ed.* **2015**, *54*, 6251–6254.

[22] Zhu, Y. P.; Liu, Y. P.; Ren, T. Z.; Yuan, Z. Y. Self-supported cobalt phosphide mesoporous nanorod arrays: A flexible and bifunctional electrode for highly active electrocatalytic water reduction and oxidation. *Adv. Funct. Mater.* **2015**, *25*, 7337–7347.

[23] Li, Y. J.; Zhang, H. C.; Jiang, M.; Kuang, Y.; Sun, X. M.; Duan, X. Ternary NiCoP nanosheet arrays: An excellent bifunctional catalyst for alkaline overall water splitting. *Nano Res.* **2016**, *9*, 2251–2259.

[24] Wang, J. H.; Cui, W.; Liu, Q.; Xing, Z. C.; Asiri, A. M.; Sun, X. P. Recent progress in cobalt-based heterogeneous catalysts for electrochemical water splitting. *Adv. Mater.* **2016**, *28*, 215–230.

[25] Pu, Z. H.; Liu, Q.; Jiang, P.; Asiri, A. M.; Obaid, A. Y.; Sun, X. P. CoP nanosheet arrays supported on a Ti plate: An efficient cathode for electrochemical hydrogen evolution. *Chem. Mater.* **2014**, *26*, 4326–4329.

[26] Liu, Y. W.; Cheng, H.; Lyu, M. J.; Fan, S. J.; Liu, Q. H.; Zhang, W. S.; Zhi, Y. D.; Wang, C. M.; Xiao, C.; Wei, S. Q. et al. Low overpotential in vacancy-rich ultrathin $CoSe_2$ nanosheets for water oxidation. *J. Am. Chem. Soc.* **2014**, *136*, 15670–15675.

[27] Wu, J.; Ren, Z. Y.; Du, S. C.; Kong, L. J.; Liu, B. W.; Xi, W.; Zhu, J. Q.; Fu, H. G. A highly active oxygen evolution electrocatalyst: Ultrathin CoNi double hydroxide/CoO nanosheets synthesized via interface-directed assembly. *Nano Res.* **2016**, *9*, 713–725.

[28] Liu, Y. W.; Xiao, C.; Lyu, M. J.; Lin, Y.; Cai, W. Z.; Huang, P. C.; Tong, W.; Zou, Y. M.; Xie, Y. Ultrathin Co_3S_4 nanosheets that synergistically engineer spin states and exposed polyhedra that promote water oxidation under neutral conditions. *Angew. Chem., Int. Ed.* **2015**, *54*, 11231–11235.

[29] Tan, C. L.; Zhang, H. Wet-chemical synthesis and applications of non-layer structured two-dimensional nanomaterials. *Nat. Commun.* **2015**, *6*, 7873.

[30] Morales-Guio, C. G.; Liardet, L.; Hu, X. L. Oxidatively electrodeposited thin-film transition metal (oxy) hydroxides as oxygen evolution catalysts. *J. Am. Chem. Soc.* **2016**, *138*, 8946–8957.

[31] Chen, P. Z.; Xu, K.; Fang, Z. W.; Tong, Y.; Wu, J. C.; Lu, X. L.; Peng, X.; Ding, H.; Wu, C. Z.; Xie, Y. Metallic Co_4N porous nanowire arrays activated by surface oxidation as electrocatalysts for the oxygen evolution reaction. *Angew.*

Chem., Int. Ed. **2015**, *54*, 14710–14714.

[32] Jiang, P.; Liu, Q.; Liang, Y. H.; Tian, J. Q.; Asiri, A. M.; Sun, X. P. A cost-effective 3D hydrogen evolution cathode with high catalytic activity: FeP nanowire array as the active phase. *Angew. Chem., Int. Ed.* **2014**, *53*, 12855–12859.

[33] Huang, Y. C.; Ye, K. H.; Li, H. B.; Fan, W. J.; Zhao, F. Y.; Zhang, Y. M.; Ji, H. B. A highly durable catalyst based on $Co_xMn_{3-x}O_4$ nanosheets for low-temperature formaldehyde oxidation. *Nano Res.* **2016**, *9*, 3881–3892.

[34] Li, Z. H.; Shao, M. F.; An, H. L.; Wang, Z. X.; Xu, S. M.; Wei, M.; Evans, D. G.; Duan, X. Fast electrosynthesis of Fe-containing layered double hydroxide arrays toward highly efficient electrocatalytic oxidation reactions. *Chem. Sci.* **2015**, *6*, 6624–6631.

[35] Yuan, C. Z.; Yang, L.; Hou, L. R.; Shen, L. F.; Zhang, X. G.; Lou, X. W. Growth of ultrathin mesoporous Co_3O_4 nanosheet arrays on Ni foam for high-performance electrochemical capacitors. *Energy Environ. Sci.* **2012**, *5*, 7883–7887.

[36] Fan, Y. Q.; Shao, H. B.; Wang, J. M.; Liu, L.; Zhang, J. Q.; Cao, C. N. Synthesis of foam-like freestanding Co_3O_4 nanosheets with enhanced electrochemical activities. *Chem. Commun.* **2011**, *47*, 3469–3471.

[37] You, Y. X.; Zheng, M. J.; Ma, L. G.; Yuan, X. L.; Zhang, B.; Li, Q.; Wang, F. Z.; Song, J. N.; Jiang, D. K.; Liu, P. J. et al. Galvanic displacement assembly of ultrathin Co_3O_4 nanosheet arrays on nickel foam for a high-performance supercapacitor. *Nanotechnology* **2017**, *28*, 105604.

[38] O'sullivan, J. P.; Wood, G. C. The morphology and mechanism of formation of porous anodic films on aluminium. *Proc. Roy. Soc. Lond. A* **1970**, *317*, 511–543.

[39] Gong, F.; Wang, H.; Xu, X.; Zhou, G.; Wang, Z. S. *In situ* growth of $Co_{0.85}Se$ and $Ni_{0.85}Se$ on conductive substrates as high-performance counter electrodes for dye-sensitized solar cells. *J. Am. Chem. Soc.* **2012**, *134*, 10953–10958.

[40] Hou, Y.; Lohe, M. R.; Zhang, J.; Liu, S. H.; Zhuang, X. D.; Feng, X. L. Vertically oriented cobalt selenide/NiFe layered-double-hydroxide nanosheets supported on exfoliated graphene foil: An efficient 3D electrode for overall water splitting. *Energ. Environ. Sci.* **2016**, *9*, 478–483.

[41] Xiong, S. L.; Yuan, C. Z.; Zhang, X. G.; Xi, B. J.; Qian, Y. T. Controllable synthesis of mesoporous Co_3O_4 nanostructures with tunable morphology for application in supercapacitors. *Chem.—Eur. J.* **2009**, *15*, 5320–5326.

[42] Gao, S.; Jiao, X. C.; Sun, Z. T.; Zhang, W. H.; Sun, Y. F.; Wang, C. M.; Hu, Q. T.; Zu, X. L.; Yang, F.; Yang, S. Y. et al. Ultrathin Co_3O_4 layers realizing optimized CO_2 electroreduction to formate. *Angew. Chem., Int. Ed.* **2016**, *55*, 698–702.

[43] Merki, D.; Fierro, S.; Vrubel, H.; Hu, X. L. Amorphous molybdenum sulfide films as catalysts for electrochemical hydrogen production in water. *Chem. Sci.* **2011**, *2*, 1262–1267.

[44] Li, H. B.; Yu, M. H.; Lu, X. H.; Liu, P.; Liang, Y.; Xiao, J.; Tong, Y. X.; Yang, G. W. Amorphous cobalt hydroxide with superior pseudocapacitive performance. *ACS Appl. Mater. Interfaces* **2014**, *6*, 745–749.

[45] Zhang, Y.; Cui, B.; Qin, Z. T.; Lin, H.; Li, J. B. Hierarchical wreath-like Au–$Co(OH)_2$ microclusters for water oxidation at neutral pH. *Nanoscale* **2013**, *5*, 6826–6833.

[46] Zhu, Y. C.; Li, H. L.; Koltypin, Y.; Gedanken, A. Preparation of nanosized cobalt hydroxides and oxyhydroxide assisted by sonication. *J. Mater. Chem.* **2002**, *12*, 729–733.

[47] Cao, B. F.; Veith, G. M.; Neuefeind, J. C.; Adzic, R. R.; Khalifah, P. G. Mixed close-packed cobalt molybdenum nitrides as non-noble metal electrocatalysts for the hydrogen evolution reaction. *J. Am. Chem. Soc.* **2013**, *135*, 19186–19192.

[48] Kuang, Y.; Feng, G.; Li, P. S.; Bi, Y. M.; Li, Y. P.; Sun, X. M. Single-crystalline ultrathin nickel nanosheets array from *in situ* topotactic reduction for active and stable electrocatalysis. *Angew. Chem., Int. Ed.* **2016**, *55*, 693–697.